Light Metals 2014
Edited by: John Grandfield
TMS (The Minerals, Metals & Materials Society), 2014

MACROSEGREGATION MODELLING OF DC-CASTING INCLUDING GRAIN MOTION AND SURFACE EXUDATION

Dag Mortensen[1], Mohammed M'Hamdi[2], Kjerstin Ellingsen[2], Knut Tveito[3], Liss Pedersen[4] and Geir Grasmo[4]
[1]Institute for Energy Technology, Kjeller, N-2027, Norway
[2]SINTEF Materials and Chemistry, Oslo, N-0314, Norway
[3]Norwegian University of Science and Technology, Trondheim, N-7034, Norway
[4]Alcoa, Lista, N-4541, Norway

Keywords: Macrosegregation, DC-casting, Modelling, Air-gap, Deformation, Exudation

Abstract

The as cast chemical composition of a DC-cast billet or slab involves mechanisms as movement of solid grains, that are lean on alloying elements, as well as movement of interdendritic liquid, that are enriched on alloying elements. These phenomena can result in the composition being out of the specification at the surface area for billets or in the centre for large slabs. In this study macrosegregation including thermal and solutal convection, solidification shrinkage, grain motion and surface exudation is simulated on a billet cast at the Alcoa Lista plant. The model includes the air-gap formation against the mould during DC-casting and the flow of liquid through the semi-solid surface that is created under such conditions. Modelling results are compared with measurements of chemical composition through the billet from centre to surface and on the exuded layer itself as well as a characterization of the thickness of the exuded layer.

Introduction

Macrosegregation in a cast product is the result of several competing phenomena. *Thermal convection* will drive the fluid flow downwards along a solidifying wall while *solutal convection* for alloys with a light alloy element (like magnesium) will drive the flow in the opposite direction. *Free moving equiaxed solid grains* are not always heavier than the enriched liquid if the alloys contain a high amount of a heavy element. *Shrinkage flow* is an important effect typically leading to a depleted zone in the centre of a DC-cast product and it might be worse of better when the other mechanisms for macrosegregation is "added". For the surface region *exudation* tend to be a dominating effect - during DC-casting of aluminium ingots the surface against the mould experiences a pull-in force that magnifies the air-gap during solidification close to the mould surface. This is a global phenomenon that results in early and large air-gap formations compared to the shape-casting situation. Due to the semi-solid surface created under such conditions, exudation through the surface may appear. Further on, *forced convection* can modify all the above mentioned mechanisms by an external controlled flow (flow distributors, electromagnetic induced, ultrasonic etc).

Due to the complexity involved a modeling tool may be very useful in quantifying the different effects for a specific alloy cast with a special design. And thereby support new process developments directed at minimizing macrosegregation.

In an earlier work [1] efforts were made to model the exudation flow, not based on a pre-set of the primary cooling zone and the position of the air-gap against the mould. Instead a more sophisticated model (called Alsim) were applied to predict the length of the primary cooling and air-gap zones as well as the thickness of the air-gap. The calculation of the thickness of the air-gap was based on displacements results from the mechanical model part. This thickness was then modified due to the filling of the gap by the enriched exuded liquid. The same coupled thermo-fluid-mechanical model is applied in the study presented here, but now a macrosegregation module has also been added to the modeling framework.

Experimental study

The investigated material was taken from a 270mm (11 inch) billet produced at Alcoa Lista. Details about the mould technology are found in [2]. The alloy composition target is shown in Table 1.

Table 1. Chemical target composition for the alloy.

Conc. [wt%]	Si	Mg	Fe	Mn	Cu
	0.63	0.46	0.23	0.17	0.15

A photograph of a typical surface of the alloy called F27 is shown in Figure 1.

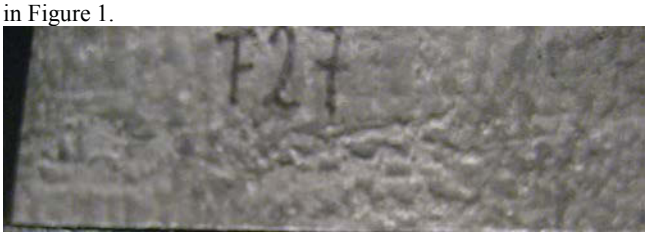

Figure 1. Photograph showing typical surface appearance.

The samples for macrosegregation characterization of the subsurface layer were made by cutting a 3mm ring from the billet, which was subsequently cut in half and straightened. Then samples of 4x4cm size were made for OES (Optical Emission Spectrography). The samples were milled in 200µm steps to obtain a detailed macrosegregation profile in the subsurface region. The bulk macrosegregation profile was made up by OES measurements every ~10mm from the surface to the centre of the billet. The measured profiles for the outer 30mm's are shown in Figure 2. The bulk macrosegregation profile for silicon is shown in Figure 3. The thickness of the exudated layer was characterized by surface topography measurements using an optical technique based on a White Light Interferometer. The measurements were carried out on a band of material (3.7x40mm). The measured surface is shown in Figure 4, while the cumulative distribution of heights in the sample are given in Figure 5. In the middle of Figure 4 we can see "beads" with a height from bottom (blue) to top (red) of about 200-300µm.

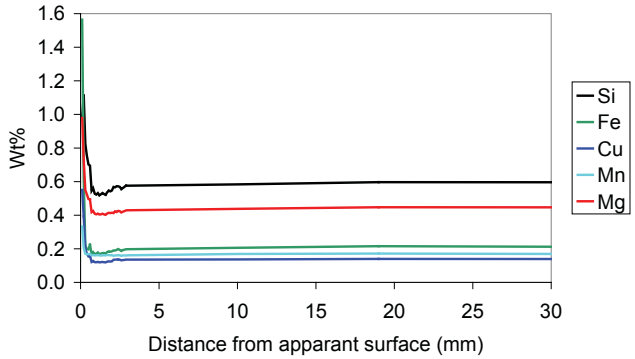

Figure 2. Measured concentration profiles for all alloy components up to 30mm from the surface.

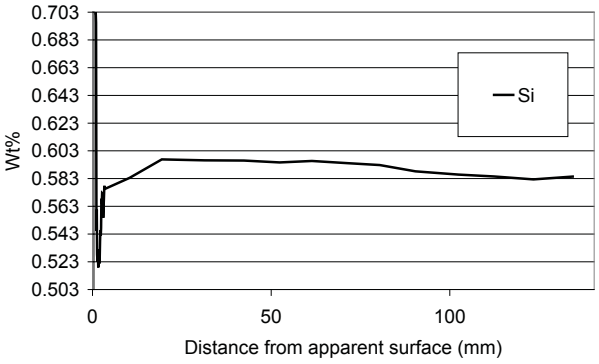

Figure 3. Measured concentration profile for silicon from surface to the centre of the billet.

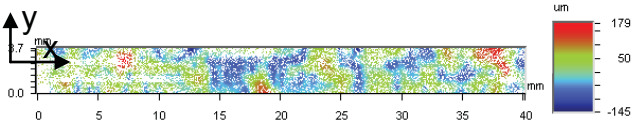

Figure 4. Measured surface topography. The height positions in the sample are given relative to the average height in each sample. The casting direction corresponds to the x-direction in the figure.

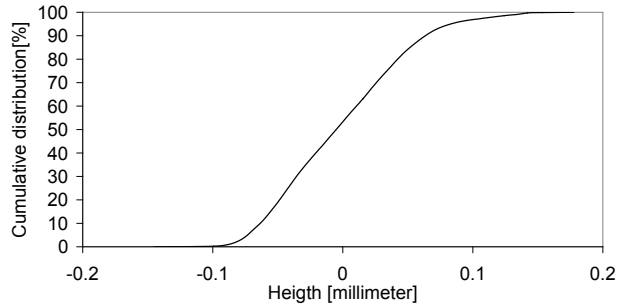

Figure 5. Cumulative distribution of the surface heights shown in Figure 4.

Modelling

In order to handle the modelling of macrosegregation, air-gap formation and exudation in a semi-solid material a volume-averaged two-phase model approach is used for the fluid flow, grain motion and the stresses and deformations. A mixture modeling approach is used for the enthalpy and species conservation. The fluid flow is divided into two different regimes, a slurry momentum regime and a porous flow regime. The slurry includes free moving grains with an average grain size dependent on the local solid volume fraction. The following equations are based on [1] modified with slurry regime momentum conservation and species conservation.

Fluid flow and grain motion

For the porous flow regime the liquid mass and momentum equations are based on the volume-averaged two-phase model in [3]:

$$\frac{D_\omega}{\partial t}\left(\rho^l g^l + \rho^s g^s\right) - \omega_j \frac{\partial}{\partial x_j}\left(\rho^l g^l + \rho^s g^s\right) + \frac{\partial}{\partial x_j}\left(\rho^l g^l u_j^l + \rho^s g^s u_j^s\right) = 0 \quad (1)$$

$$\begin{aligned} &\frac{D_\omega g^l u_i^l}{\partial t} - \omega_j \frac{\partial g^l u_i^l}{\partial x_j} + \frac{\partial g^l u_i^l u_j^l}{\partial x_j} = -\frac{g^l}{\rho^l}\frac{\partial p^l}{\partial x_i} + \\ &\frac{\partial}{\partial x_j}\nu\left(\frac{\partial g^l u_i^l}{\partial x_j} + \frac{\partial g^l u_j^l}{\partial x_i} - u_i^s \frac{\partial g^l}{\partial x_j} - u_j^s \frac{\partial g^l}{\partial x_i}\right) + \\ &\frac{g^l}{\rho^l} f_i^l - \frac{g^l \nu}{K}\left(g^l u_i^l - g^l u_i^s\right) + u_i^s\left(\frac{\partial g^l}{\partial t} - \omega_j \frac{\partial g^l}{\partial x_j} + \frac{\partial g^l u_j^l}{\partial x_j}\right) \end{aligned} \quad (2)$$

where ρ^l, ρ^s, g^l, g^s, ω_j, u_j^l, u_j^s, p^l, ν, f_i^l and K are liquid density, solid density, liquid volume fraction, solid volume fraction, velocity of computational nodes, liquid velocity, solid velocity, liquid pressure, kinematic viscosity, external forces and permeability, respectively. $D_\omega/\partial t$ denotes the time derivative of a variable moving with the velocity of the computational grid. Solidification shrinkage, interfacial friction, momentum transfer due to phase change and macroscopic viscous stress contribution are included. The permeability of the semi-solid material is assumed to follow the Kozeny-Carman relation:

$$K = \frac{l_m^2}{180}\frac{g_l^3}{(1-g_l)^2} \quad (3)$$

where l_m is a characteristic length of the microstructure. In our case, with a grain-refined close to globulitic microstructure the arithmetic mean of the measured average grain size and secondary dendrite arm spacing close to the surface was used. This was 120μm and 30μm respectively, so 75μm was used to represent l_m.

For the solid free grain (slurry) regime, following [4], a similar equation like Eq.2 may be defined and simplified by neglecting the inertia term (solid grains are instantaneous accelerated by the liquid), and using that the solid particles are completely surrounded by liquid with pressure p^l we end up with the following solid momentum conservation equation:

$$-\frac{g^s}{\rho^s}\frac{\partial p^l}{\partial x_i} + \frac{g^s}{\rho^s} f_i^s + \frac{\rho_l}{\rho_s} D\left(g^l u_i^l - g^l u_i^s\right) = 0 \quad (4)$$

where D is a drag term for the free grain regime, see [4]. In this study a constant solid volume fraction (packing fraction) is used to distinguish between the slurry and the porous regime. For solid volume fractions smaller than the packing fraction the slurry

regime is applied. In the porous regime (solid volume fraction larger than the packing fraction) the solid velocity is set equal to the casting velocity. The numerical solution applies in principle the same techniques as in [5].

Stresses and deformations

The mechanical analysis is carried out in the fully solid regions of the ingot as well as in the coherent part of the mushy zone. The upper boundary of the coherent mushy zone corresponds to a solid volume fraction equal to 0.6 in this study. For a complete description of the mechanical model employed, see [6]. Here only a brief description is provided. Denoting the solid stress σ_s, the mixture momentum balance in the coherent part of the mushy zone can be expressed by:

$$\nabla \cdot \left[g_s \boldsymbol{\sigma}_\mathbf{s}\right] - \nabla\left[g_l \mathbf{p}_\mathbf{l}\right] + \left[\boldsymbol{\rho}_\mathbf{s}\mathbf{g}_\mathbf{s} + \boldsymbol{\rho}_\mathbf{l} g_l\right]\mathbf{g} = \mathbf{0} \qquad (5)$$

where **g** is the gravity vector. The model formulation has been based on the classical small deformation theory where the total strain e, derivable from the displacement field u is subdivided into viscoplastic, elastic and thermal components.

$$\boldsymbol{\varepsilon} = \frac{1}{2}\left(\nabla \mathbf{u} + \left[\nabla \mathbf{u}\right]^t\right) = \boldsymbol{\varepsilon}^{vp} + \boldsymbol{\varepsilon}^e + \boldsymbol{\varepsilon}^T \qquad (6)$$

The thermal strain component can be written as an integral of the (volumetric) thermal expansion coefficient β_T.

$$\boldsymbol{\varepsilon}^T = -\frac{1}{3}\int_T^{T_{coh}} \beta_T(T)dT \cdot \mathbf{I} \qquad (7)$$

The constitutive equation for elasticity (Hook's law) defines how the stress depends on the elastic strain $\boldsymbol{\varepsilon}^e$ and the temperature dependent Young's modulus and Poisson's ratio entering the matrix **D**.

$$\boldsymbol{\sigma} = \mathbf{D}(T) \cdot \boldsymbol{\varepsilon}^e \qquad (8)$$

Constitutive equations for the viscoplastic deformation of aluminium alloys during solidification are based on [7], where the mushy zone is considered as a partially cohesive porous solid saturated with liquid:

$$\dot{\boldsymbol{\varepsilon}}_s^p = \frac{\dot{\varepsilon}_0 e^{-\frac{Q}{RT}}}{\left(C\sigma_0\right)^n}\left[-\frac{1}{9}A_2(g_s)J_1\mathbf{I} + \frac{3}{2}A_3(g_s)g_s\boldsymbol{\tau}_s\right]\left[\frac{1}{9}A_2(g_s)J_1^2 + 3A_3(g_s)J_2\right]^{\frac{n-1}{2}} \qquad (9)$$

$$\dot{C} = \alpha(g_s, X)\left(1 - \frac{C}{C^*(g_s, X)}\right)\dot{\bar{\varepsilon}}_s^p \qquad (10)$$

J_1 and J_2 are the first and second invariants of the effective stress tensor $\hat{\boldsymbol{\sigma}}_s = (g_s\boldsymbol{\sigma}_s - g_l p_l \mathbf{I}) + p_l \mathbf{I}$, $\boldsymbol{\tau}_s$ is the solid deviatoric stress tensor, $\dot{\bar{\varepsilon}}_s^p$ is the effective strain rate, and X is the stress triaxiality. Equation (10) describes the evolution of the partial cohesion of the coherent mushy zone. Expressions for the solid fraction and triaxiality dependent functions, A_2, A_3, and C* are all given in [6]. In the fully solid regions (g_s=1, A_2=0, A_3=1, C=1), equation (5) simplifies to the usual Cauchy's equation for a fully solid material

$$\nabla \cdot \boldsymbol{\sigma}_\mathbf{s} + \boldsymbol{\rho}_\mathbf{s}\mathbf{g} = \mathbf{0} \qquad (11)$$

A set of equations assuming steady state creep above a temperature T_0 and work hardening below this temperature, are applied for viscoplastic deformation in the fully solidified regime:

$$\bar{\sigma} = F(T) \cdot \left(\phi_0 + \phi\right)^{n(T)} \cdot \left(\dot{\bar{\varepsilon}}_p\right)^{m(T)} \qquad (12)$$

$$d\phi = \begin{cases} d\bar{\varepsilon}_p & \text{when} \quad T \le T_0 \\ 0 & \text{when} \quad T > T_0 \end{cases} \qquad (13)$$

Enthalpy and species conservation

The following mixture formulation is applied:

$$\frac{D_\omega}{\partial t}(\rho h) - \omega_j \frac{\partial}{\partial x_j}\left(\rho^l g^l h^l + \rho^s g^s h^s\right) + \frac{\partial}{\partial x_j}\left(\rho^l g^l h^l u_j^l + \rho^s g^s h^s u_j^s\right) = \frac{\partial}{\partial x_j}\lambda\frac{\partial}{\partial x_j}T \qquad (14)$$

where h, λ and T are the enthalpy, the heat conductivity and the temperature. In the macrosegregation calculation the temperature is found from an iterative micro model dependent on the mixture enthalpy and the mixture concentration (i.e. a non-fixed solidification path is applied). The lever rule model was applied in this study. Constant liquidus slope and partition coefficient for silicon was -6.7K/wt% and 0.13, respectively, from [8]. For the other alloy components is was -1.7/-1.4/-5.5/-2.6wt% and 0.02/0.95/0.35/0.14 for Fe/Mn/Mg/Cu, respectively.

For the solute a similar mixture formulation is used:

$$\frac{D_\omega}{\partial t}\left(\rho^l g^l c_i^l + \rho^s g^s c_i^s\right) - \omega_j \frac{\partial}{\partial x_j}\left(\rho^l g^l c_i^l + \rho^s g^s c_i^s\right) + \frac{\partial}{\partial x_j}\left(\rho^l g^l c_i^l u_j^l + \rho^s g^s c_i^s u_j^s\right) = \frac{\partial}{\partial x_j}\rho^l g^l D_i^l \frac{\partial}{\partial x_j}c_i^l + \frac{\partial}{\partial x_j}\rho^s g^s D_i^s \frac{\partial}{\partial x_j}c_i^s \qquad (15)$$

By using the definitions $\rho c^i = \rho^l g^l c_i{}^l + \rho^s g^s c_i{}^s$ and $\rho D^i = \rho^l g^l D_i{}^l + \rho^s g^s D_i{}^s$ and taking into account that the diffusion is very small this equation can be approximated with the following simplification:

$$\frac{D_\omega}{\partial t}(\rho c_i) - \omega_j \frac{\partial}{\partial x_j}\left(\rho^l g^l c_i^l + \rho^s g^s c_i^s\right) + \frac{\partial}{\partial x_j}\left(\rho^l g^l c_i^l u_j^l + \rho^s g^s c_i^s u_j^s\right) = \frac{\partial}{\partial x_j}\rho D_i \frac{\partial}{\partial x_j}c_i \qquad (16)$$

Diffusion constants applied in this study was 10^{-8}m^2/s and 10^{-12}m^2/s for the liquid and the solid, respectively (all alloy components).

Thermo-fluid-mechanical coupling

The resulting stresses and displacements affect the thermal boundary conditions regarding contact zones or air gaps between ingot and mold. Fluid outflow from the semi-solid surface is only allowed if there is a local air-gap at the current element surface. The local air-gap value is a result of the local displacements and the local exudation thickness (a large outflow will close the air-gap). With no air-gap the fluid outflow is hindered by the solid mould surface. Due to numerical considerations of what to be handled as a real air-gap the minimum air-gap size for exudation was set to 1 micrometer in this study. If the calculated air-gap is larger than 1μm a pressure boundary condition is applied in the solution of the liquid mass and momentum equations. The pressure at the melt surface is equal to zero and the pressure at the local air-gap surface is calculated from the height of the metal column above the surface. This pressure drop is then the driving

force for the fluid outflow, while the pressure drop through the semi-solid material is the limiting factor. More details about thermal and mechanical boundary conditions can be found in [2].

Material properties

Thermal properties for the alloy were calculated by the microstructure model Alstruc [9]. For the mechanical properties the F(T), n(T) and m(T) functions in equation (12) were taken from the 6063-alloy in [10]. The parameters for the cohesion mechanical model of the semi-solid material were taken from [7], as measured for a grain-refined AlCu-alloy.

Results

A fully coupled heat and fluid flow, stresses and deformation calculation was performed. This simulation included the ingot, the starting block, the mould, the gas, oil and insulation (transition) rings above the mould and the hot-top. The contact area and the air-gap size against the mould were dynamically calculated by the model and back-coupled to the thermal boundary conditions. Elements are added to the computational domain as the simulation proceeds so the domain increases in size similar to the casting itself. Thereby the concentration fields are calculated for the whole start-up phase. The calculated silicon concentration at 220 seconds from start of casting is shown in Figure 6.

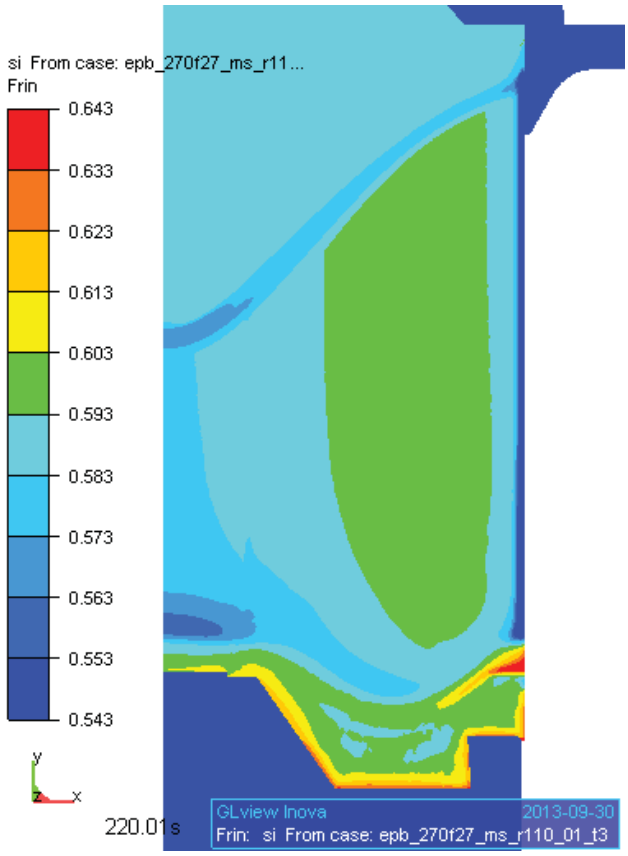

Figure 6. Silicon concentrations (wt%) in the billet at 220 seconds from start of casting.

The average silicon concentration calculated from the measurements was 0.593wt%. The "warm" colours (green, yellow, red etc) represent areas with positive segregation while the "cold" colours (the blue ones) represent areas with negative segregation. Due to shrinkage flow the average concentrations inside the mushy sone is negative. The concentration within the exuded layer is of course much higher, this concentration was calculated to be 2.56wt% and the thickness of the exuded layer was 0.11mm. Figure 7 shows a focused view of the mushy zone close to the mould.

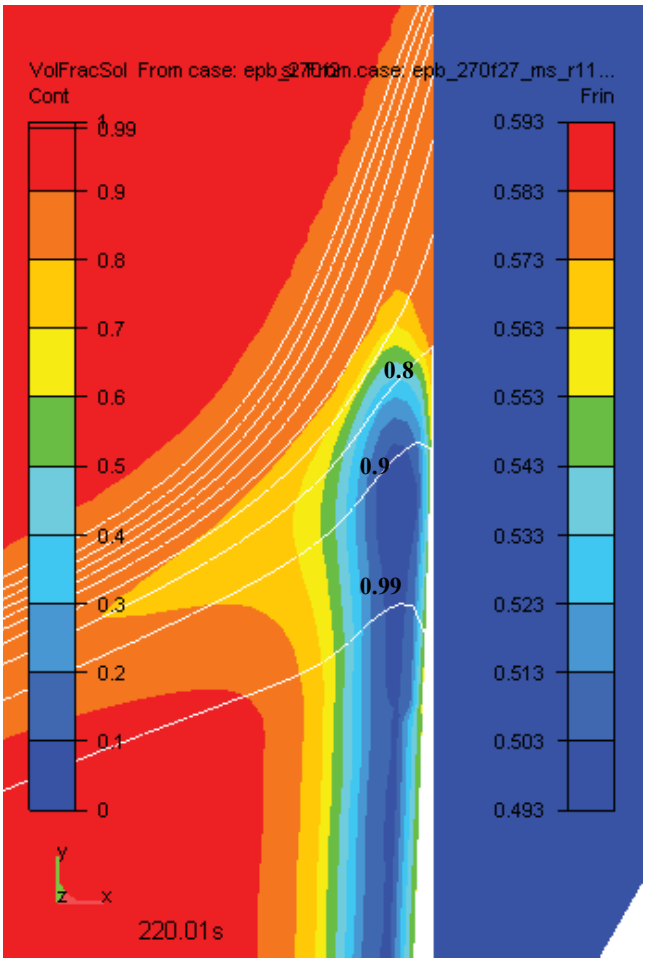

Figure 7. Silicon concentrations (wt%) in the billet at 220 seconds from start of casting. Focused view at the surface region.

Note how the solid fraction varies close to the surface for higher values where exudation is present (e.g. 0.9 and 0.99 in Figure 7). This is due to the variation in the local chemical composition resulting in different solidification paths.

The calculated silicon concentration profile through the billet at close to stationary conditions is shown in Figure 8. Figures 9, 10, 11 and 12 shows the similar profile but after removing, one by one, the mechanisms behind macrosegregation, but keeping exudation. The scale has been changed in order to better show the differences.

Figure 13 shows an ad-hoc variation of grain size and how that influences the results for modeling cases including grain motion, shrinkage etc but without exudation. Exudation was removed in order to better study the effect of grain size alone. The packing

fractions of the grains were also varied such that the packing fraction was reduced with larger grain sizes and increased with smaller grain sizes.

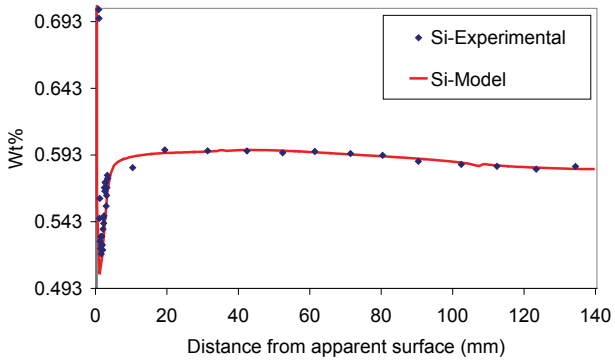

Figure 8. Comparison between measured silicon concentrations (diamond symbols) and model results (continuous line).

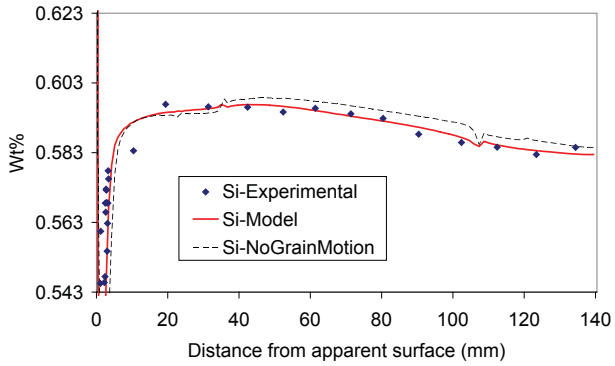

Figure 9. Comparison between measured silicon concentrations (diamond symbols) and model results (continuous line) and simplified model results with no grain motion (dotted line).

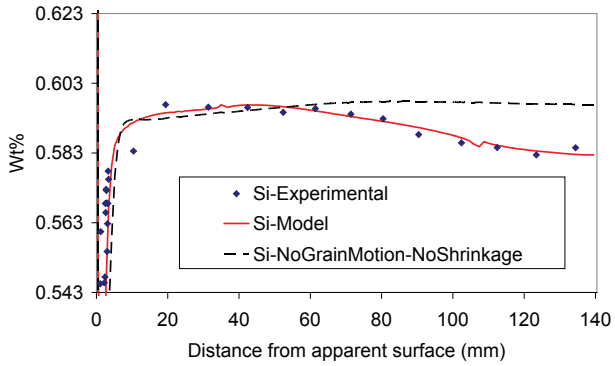

Figure 10. Comparison between measured silicon concentrations (diamond symbols) and model results (continuous line) and simplified model results with no grain motion and no shrinkage flow (dotted line).

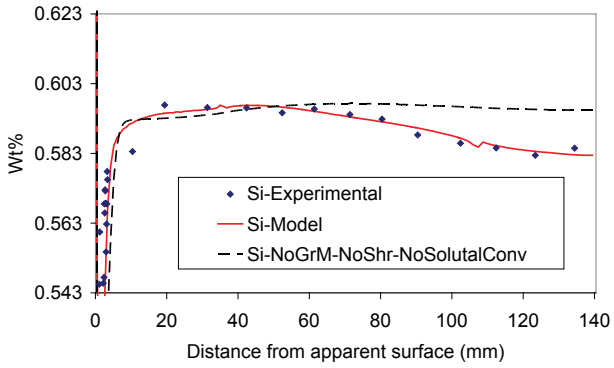

Figure 11. Comparison between measured silicon concentrations (diamond symbols) and model results (continuous line) and simplified model results with no grain motion, no shrinkage flow and no solutal convection (dotted line).

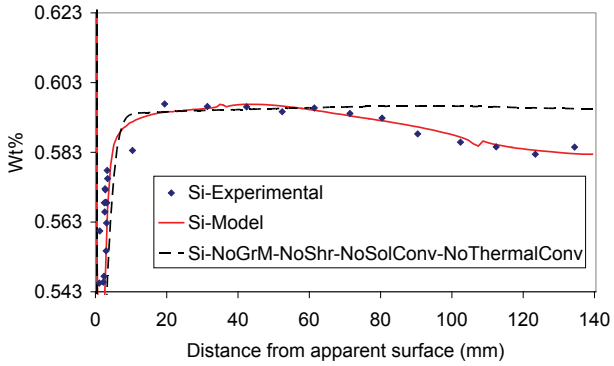

Figure 12. Comparison between measured silicon concentrations (diamond symbols) and model results (continuous line) and simplified model results with no grain motion, no shrinkage flow, no solutal convection and no thermal convection (dotted line).

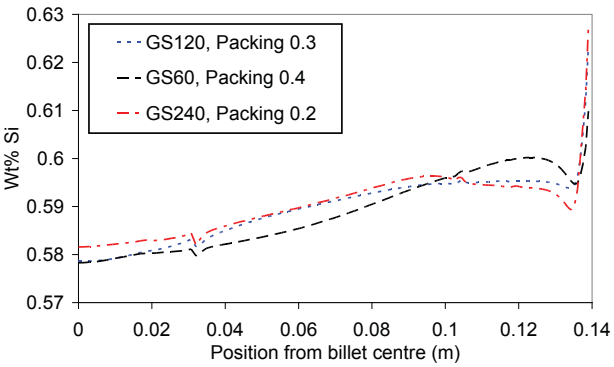

Figure 13. Model results where exudation was omitted. Results are with grain size 60μm and solid volume fraction at packing 0.4, grain size 120μm and packing fraction 0.3, grain size 240μm and packing fraction 0.2.

Discussion

From Figure 5, we can see that about 95% of the surface is in the interval –0.1mm to +0.1mm from an average level, but we do not know from these measurements the position of the original

surface. If we assume that the original surface correspond to -0.1mm in Figure 5 the average exudation thickness should be around 0.1mm. The calculated exudation thickness 0.11mm is of that order. So both the surface segregation profile and the exudation thickness are supported by the measurements. Also comparing the calculated average concentration in the 0.11mm thick exudated layer, which was 2.56wt%, with the depleted profile in the subsurface layer shows a close match between this profile and the amount of exuded silicon.

The bulk macrosegregation profile is of interest regarding validation of the modelling tool. The depleted centre region is found also in the model and of the same order. Looking on the 2D map of concentrations in Figure 6 we may notice the positive segregation close to the bottom block and the mould which is due to solidification shrinkage against a chill surface (if exudation is not present). Due to a filling time and initial solidification before start of casting the impression of the transition ring can also be seen in the concentration map about 20mm up from the bottom block edge. As the casting starts (bottom block starts to move) the continuous casting enhanced air-gap is developing and so is the exudation.

Looking on the results in Figures 9 to 12 shows that shrinkage flow is the main contribution to the bulk macrosegregation for this particular example. Removing grain motion decreases the amount of negative segregation in the centre, this is due to the removal of the lean grains transported against the centre by gravity forces. Also the depleted layer is a bit broader without grain motion, this is because the free flow down to packing (solid) fraction 0.3, when grain motion is included, narrows the zone with restricted inter-dendritic flow. If the shrinkage flow is removed in addition to grain motion there is not much bulk macrosegregation left. There is a small positive segregation downwards along the solidification front due to the transport of enriched interdendritic liquid. For this transport thermal convection is more important than solutal convection, this is probably due to the low alloy content and including magnesium as well which diminishes the solutal forces. Removing also thermal convection (so only forced convection and exudation left) shows a uniform bulk concentration profile.

The results regarding sensitivity of grain size show that assuming half grain size (more globulitic and flowing freely deeper into the mushy zone) enhances the negative segregation in the centre while assuming double grain size (more dendritic and packing at smaller solid fracion) diminishes the negative centre segregation. Against the mould (which act as a normal chill surface in this case without exudation) the positive segregation is caused by shrinkage flow.

The risks (uncertainties) in a modelling study of this kind are numerous. Factors influencing the results are physical constants like phase diagram data, partition coefficients, the length parameter used for calculation of the permeability, choice of drag coefficient, microsegregation model etc. In order to gain confidence in a model like this a set of macrosegregation profiles for different DC-cast products (dimensions, alloys) are needed. Some of them can be found in the literature, like in [11]. Further work will be concentrated on validation against larger experimental data sets.

Conclusions

The macrosegregation in the case of a Ø270mm 6xxx billet is mainly due to exudation and shrinkage flow. Grain motion and solutal convection plays a smaller role. This is not a general result but a result for this particular alloy, dimension and casting technique. The amount of exudation can be influenced by the metallostatic head and the mould cooling height, while negative centre segregation from shrinkage flow can chiefly be influenced by the casting speed. Modelling of macrosegregation can contribute to enhanced understanding and control of cast product quality and homogeneity in general.

Acknowledgements

Funding of this work by the MINAC-project (Modelling assisted Innovation for the Aluminium DC Casting process) is gratefully acknowledged. Partners in MINAC were Alcoa Norway ANS, Aleris Rolled Products Germany GmbH, Hydro Aluminium ASA, Materials innovation institute (M2i), Stiftelsen SINTEF and Institute for Energy Technology (IFE). The project was supported by the Norwegian research council through the BIA programme.

References

[1] D. Mortensen, B.R. Henriksen, M. M'Hamdi and H.G. Fjær, "Coupled modelling of air-gap formation and surface exudation during extrusion ingot DC-casting", Light Metals 2008, TMS, Warrendale PA, pp 773-779.

[2]] D. Mortensen, B.R. Henriksen, J. Hvistendahl, H.G. Fjær, "Modelling of mould toe-in during extrusion ingot DC-casting", Light Metals 2007, TMS, Warrendale PA, pp715-720.

[3] J. Ni and C. Beckermann, "A volume-averaged two-phase model for transport phenomena during solidification", Metall. Trans. B, 1991, vol.22B, pp.349-361.

[4] M. Založnik, H. Combeau, "An operator splitting scheme for coupling macroscopic transport and grain growth in a two-phase multiscale solidification model: Part I – Model and solution scheme", Comp. Mat. Sci. 48 (2010), pp.1-10.

[5] D. Mortensen, "A mathematical model of the heat and fluid flows in direct-chill casting of aluminium sheet ingots and billet", Metall. Trans. B, 1999, vol.30B, pp.119-133.

[6] M. M'Hamdi, A. Mo and H.G. Fjær, "TearSim: A two-phase model addressing hot tearing formation during aluminium direct chill casting", Metall. Trans. A, 2006, vol.37A, pp.3069-3083.

[7] O. Ludwig, Ph.D. Thesis, Institut National Polytechnique de Grenoble, Grenoble, Feb. 2004.

[8] M.A. Kearns and P.S. Cooper, "Effects of solute interactions on grain refinement of commercial aluminium alloys", Light Metals 1997, TMS, Warrendale PA, pp655-661.

[9] A.L. Dons et.al., Metall. Trans. A, 1999, vol.30A, pp.2135-2146.

[10] W.M. van Haaften, "Constitutive behaviour and hot tearing during aluminium DC casting", PhD-Thesis TUDelft, The Netherlands, 2002. ISBN 90-9015792-1.

[11] L. Zhang, D.G. Eskin, A. Miroux, T. Subroto and L. Katgerman, "Effect of inlet geometry on macrosegregation during the direct chill casting of 7050 alloy billets. Experiments and computer modelling", Mat.Sci. and Eng. 33, 2012, IOP Conf.Series 012019.